

## CONDITIONS OF CHLORITE GROWTH IN THE HILL END GOLDFIELD, NEW SOUTH WALES, AUSTRALIA: SOME PREDICTIONS AND EVALUATIONS

JIANCHUN LU

*School of Earth Sciences, The University of Melbourne, Parkville, VIC 3052, Australia*

PHILIP K. SECCOMBE

*Department of Geology, The University of Newcastle, Callaghan, NSW 2308, Australia*

JOHN L. WALSHE

*Department of Geology, Australian National University, Canberra, ACT 2601, Australia*

### ABSTRACT

A solid-solution model for the composition of chlorite has been used to calculate the physicochemical conditions of gold deposition for the slate-belt-hosted Hill End goldfield in the Paleozoic Lachlan Fold Belt of New South Wales, Australia. A P–T range of 295–340°C and 1.4–3 kbar, and the redox conditions for three major stages of gold mineralization, are estimated by combining data for T,  $f(\text{O}_2)$  and  $f(\text{S}_2)$ , calculated from chlorite compositions, with the results obtained from fluid-inclusion analyses and a knowledge of the mineral paragenesis. Gold deposition occurred in a redox environment where  $f(\text{O}_2)$  ranged from  $10^{-32}$  to  $10^{-36.4}$ , tracked by fluid and mineral species from below the  $\text{CO}_2$ – $\text{CH}_4$  stability boundary to above the pyrite–pyrrhotite stability boundary, respectively. The temperature corrections to fluid-inclusion  $T_h$  data provided by the chlorite model could be as high as 190°C. With careful paragenetic control, the chlorite geothermometer seems to be a powerful tool in deciphering multistage fluid systems, and offers a solution to some of the ambiguities attending fluid-inclusion studies in metamorphic environments.

*Keywords:* chlorite composition, gold mineralization, temperature,  $f(\text{O}_2)$ , pH, Hill End goldfield, New South Wales, Australia.

### SOMMAIRE

Nous avons utilisé un modèle de solution solide conçu pour exprimer la composition de la chlorite afin de déterminer les conditions physicochimiques de déposition de l'or dans le champ aurifère de Hill End, dans la ceinture d'ardoise plissée de Lachlan, d'âge paléozoïque, au Nouveau Pays de Galles, en Australie. Nous en déduisons un intervalle de température entre 295° et 340°C à une pression comprise entre 1.4 et 3 kbar. Nous spécifions les conditions d'oxydation au cours des trois stades de minéralisation en regroupant les données sur T,  $f(\text{O}_2)$  et  $f(\text{S}_2)$  calculées à partir de la composition de la chlorite avec les résultats d'analyses des inclusions fluides et une connaissance des associations paragenétiques. La déposition de l'or a eu lieu dans un milieu marqué par une fugacité d'oxygène entre  $10^{-32}$  et  $10^{-36.4}$ , tel que le montrent la spéciation de la phase fluide et les minéraux coexistants, d'une condition inférieure à l'équilibre  $\text{CO}_2$ – $\text{CH}_4$  jusqu'à une condition supérieure à l'équilibre pyrite–pyrrhotite, respectivement. Les corrections à la température à partir des valeurs  $T_h$  des inclusions fluides pourraient atteindre 190°C. Avec un contrôle serré des associations paragenétiques, le géothermomètre fondé sur la chlorite semble offrir un outil puissant pour décortiquer les systèmes à plusieurs étapes d'incursion de fluide, et résoudre certaines des ambiguïtés rencontrées dans les études d'inclusions fluides dans les milieux métamorphiques.

(Traduit par la Rédaction)

*Mots-clés:* composition de la chlorite, minéralisation en or, température,  $f(\text{O}_2)$ , pH, champ aurifère de Hill End, Nouveau Pays de Galles, Australie.

## INTRODUCTION

The Hill End goldfield, in New South Wales, Australia, is an example of a syntectonic, slate-belt-hosted gold deposit of Paleozoic age (Fig. 1). Bedding-parallel auriferous quartz veins are hosted by a deformed sequence of metagreywacke and slate of Silurian-Devonian age, developed within the North Hill End Trough, a post-Middle Silurian pull-apart basin that formed between two segments of an Ordovician and Early Silurian volcanic island arc in the eastern part of the Lachlan Fold Belt of southeastern Australia (Packham 1969, Scheibner 1973).

Structural observations (Seccombe & Hicks 1989, Windh 1990, Lu & Seccombe 1993, Seccombe *et al.* 1993) indicate that individual veins formed over a protracted period corresponding to the major event of deformation (Early Carboniferous: Powell & Edgecombe 1978). The fluid-inclusion study of Lu & Seccombe (1993) revealed that some of the primary inclusions from early generations of quartz show features of re-equilibration under conditions of internal underpressure, which suggests trapping prior to the peak of metamorphism. Under these circumstances, temperatures of homogenization obtained from fluid-inclusion studies are not a useful guide to the tempera-

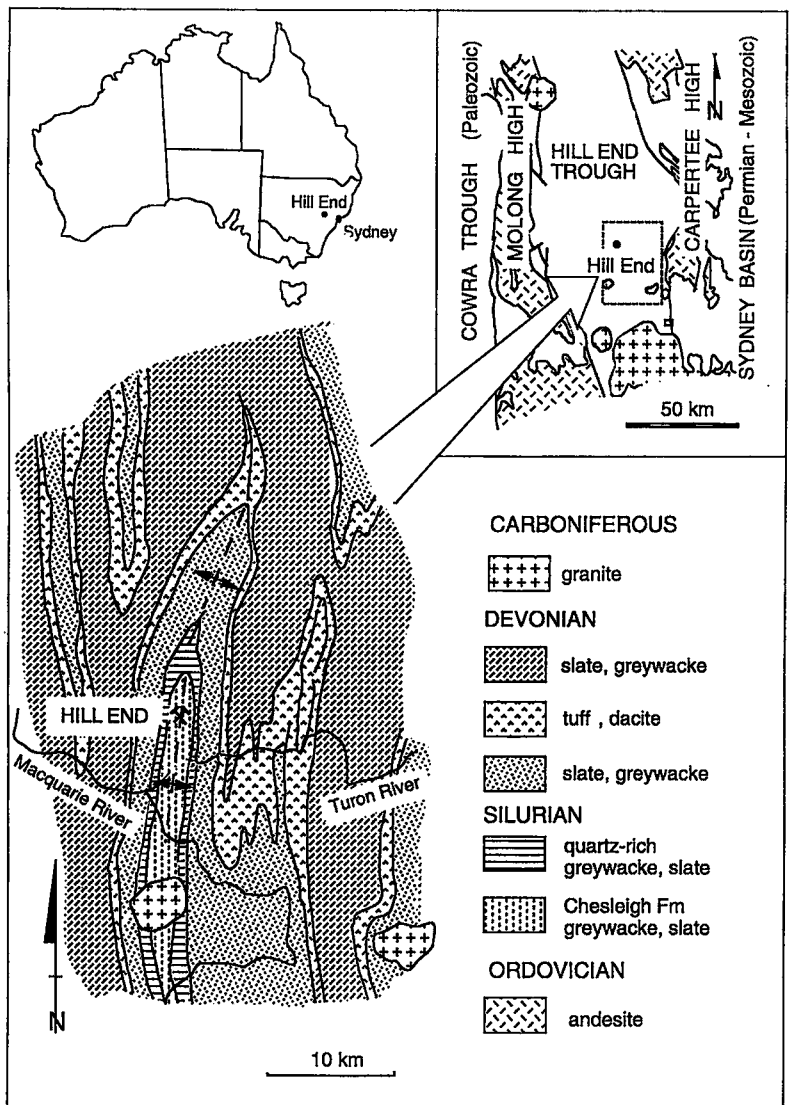


FIG. 1. Regional geology of the North Hill End Trough, and location of mineralized districts. Geology compiled from New South Wales Geological Survey map sheets Bathurst and Dubbo (scale: 1:250,000).

tures of trapping of the fluid. Therefore, the results of the fluid-inclusion study cannot be used directly to trace the conditions of mineralization, especially for events early in the paragenesis of the gold veins. This paper is designed to reconstruct the P-T regime during mineralization by combining the results of the fluid-inclusion study with information on temperature and the fugacity of oxygen and sulfur obtained from the chlorite solid-solution model of Walshe (1986). Details of the approach and the source of data used in the calculations are available in Walshe (1986).

The well-constrained paragenesis and the intimate relationship between chlorite and gold in the veins at Hill End mean that the compositional variation of chlorite can provide important constraints on the physicochemical conditions of mineralization. The use of chlorite geothermometry is particularly relevant to Hill End, where, because of the effects of re-equilibration of fluid inclusions in early-stage fluids, and the need to apply temperature corrections to raw data on homogenization temperature ( $T_h$ ) owing to lithostatic load, temperature data obtained by fluid-inclusion analysis are difficult to interpret.

#### GEOLOGICAL BACKGROUND

Sets of gold-bearing veins are hosted by the Late Silurian Chesleigh Formation (Fig. 1), which forms the core of the Hill End anticline. Exploited veins in the central part of the mining field were found to range in width from 5 cm to 10 m, and the grades, to vary dramatically from 12 g/t to 30 kg/t (Harper 1918). The richest portions of the veins are developed on the eastern limb of the Hill End anticline. Gold has a patchy distribution within the veins; the highest grades are confined to steeply S-plunging shoots that are perpendicular to the generally N-plunging boudin and fold axes. Rocks in the vicinity of Hill End have experienced biotite-grade greenschist-facies regional metamorphism (Smith 1969, Prendergast 1981, Offler & Prendergast 1985). Peak P-T conditions of metamorphism were estimated to be 2.9 kbar and 420°C by Seccombe & Hicks (1989) on the basis of silica content of metamorphic white mica and the composition of coexisting syntectonic calcite and ferroan-magnesian calcite from the wallrocks. Structures in the Hill End Trough are characterized by a north-trending regional grain imparted by steep cleavage, (near) upright folds and contractional faults. The timing of the major deformation affecting the central parts of the Hill End Trough is not well established. Conclusions extrapolated from studies on the eastern margin of the trough (Powell 1976, Powell & Edgecombe 1978) suggest that the principal cleavage-forming event occurred during early Carboniferous time. At Hill End, folds trend northerly, and axial surfaces are upright. A well-developed axial plane cleavage strikes 170° and dips 80°E in the mine area.

#### MINERALIZED QUARTZ VEINS

Mineralized veins are bedding-parallel, and their geometry follows that of the Hill End anticline. The veins predominantly comprise quartz, carbonates and muscovite, associated with minor pyrrhotite, pyrite and marcasite and rare gold, chalcocopyrite, sphalerite and galena. On the basis of well-defined micro-scale textures developed in the vein minerals, five stages of vein and ore formation have been inferred during the development of the auriferous quartz veins (Table 1). A detailed description of the vein mineralogy is given in Lu & Seccombe (1993). Three generations of chlorite have been identified in the vein paragenesis (Stages III-V), following two periods of deposition of barren quartz (Stages I and II). Gold accompanies each of the generations of chlorite.

The first generation of vein chlorite (Stage III) is developed as fine-grained, anhedral aggregates, distributed along the vein laminations and thus parallel to vein walls.

Stage-IV chlorite forms fine- to medium-grained, anhedral to subhedral grains, which are confined to muscovite-bearing microveinlets developed oblique to the vein laminations. In this setting, chlorite is commonly associated with sulfides, and some medium- to coarse-grained Stage-IV calcite. Replacement and recrystallization textures observed in Stage-IV chlorite may be correlated with the last event (Stage V).

Stage-V chlorite consists of medium- to coarse-grained, euhedral clusters of grains associated with Stage-V quartz and Stage-V calcite to form quartz + chlorite + calcite aggregates or irregular veins. This generation of chlorite is encountered in some samples of the bedding-parallel veins, where it overgrows all earlier generations of quartz, muscovite and chlorite. Apart from the quartz veins, chlorite is also identified in the altered greywacke close to the contacts with slate, where development of silicification, chloritization, and also some sulfides including pyrrhotite and pyrite, has been noted.

TABLE 1. PARAGENESIS AND FLUID-INCLUSION DATA, HILL END GOLDFIELD, NEW SOUTH WALES, AUSTRALIA

Paragenetic stage	Mineral assemblage	$T_h$ of fluid inclusions
Stage I	quartz, (arsenopyrite?)*	280°-350°C
Stage II	quartz, muscovite, pyrrhotite.	230°-280°C
Stage III	quartz, muscovite, chlorite, pyrrhotite, calcite, sphalerite, galena, chalcocopyrite, gold.	190°-250°C
Stage IV	muscovite, chlorite, calcite, pyrrhotite, pyrite, sphalerite, galena, chalcocopyrite, gold.	150°-250°C
Stage V	quartz, chlorite, pyrrhotite, pyrite, gold.	150°-210°C

Summarized from Lu & Seccombe (1993).

\* arsenopyrite only found in alteration zone of the mineralized veins

Gold and sulfide mineralization postdate the major stage of quartz vein formation. In these veins, gold is associated with muscovite, chlorite, calcite and sulfides. Three episodes of gold deposition have been identified. The first episode of gold mineralization commenced during Stage III, whereas the second episode occurs during Stage IV. The final deposition of gold (Stage V) postdates the development of internal laminations in the major bedding-parallel veins.

Laser-Raman microprobe analysis of the inclusions indicates that gas-phase compositions relate to the paragenetic stage of the host quartz (Lu & Seccombe 1993). In Stage-I quartz,  $H_2O_{(g)}$  and  $N_2$  dominate in the primary inclusions,  $CH_4$  and  $CH_4 + H_2O_{(g)}$  are important in secondary inclusions related to mineralization, but  $H_2O_{(g)}$  is the only major phase in post-mineralization secondary inclusions. In Stage-II quartz, the composition of the gas phase is dominated by  $CH_4$  and  $CH_4 + H_2O_{(g)}$ . Earliest Stage-V quartz, associated with further deposition of gold and the formation of conformable and discordant veins of chlorite and calcite in the footwall of the principal laminated veins, contains fluid inclusions dominated by  $H_2O_{(g)}$  and  $CH_4 + H_2O_{(g)}$ . Later deposition of Stage-V quartz, accompanied by calcite in the crest of the major anticline, is characterized by  $CO_2$ -rich inclusions bearing liquid  $CO_2$ .

#### CHLORITE COMPOSITIONS: INTERPRETATION AND EVALUATION

Numerous attempts have been made to interpret the compositions of chlorite in terms of temperature of formation (see recent review by De Caritat *et al.* 1993). None of these approaches has been entirely successful.

The problem is our poor understanding of the solid-solution properties of the mineral. Other questions, such as the effect of poor microprobe analyses, are much less significant. One of the main difficulties concerns the fact that the silicon content of the mineral is not a unique function of temperature and may be strongly influenced by the pH of the environment of growth. The Walshe (1986) geothermometer seems to operate best in the range 250 to 300°C in neutral to slightly acidic environments (coexistence with sericite but not pyrophyllite or K-feldspar). These conditions are met in this study. Details of the approach and the source of data used in the calculations are available in Walshe (1986).

The samples chosen for analysis were collected either from the underground mines or from drill core. Minerals prepared for analysis include not only all three generations of vein chlorite, but also chlorite in the altered greywacke. Selected samples of rock were prepared as polished thin sections, and chlorite was described under the microscope on the basis of occurrence and paragenesis. The analyses were done at the University of Newcastle using a JSM-840 scanning electron microscope coupled with an energy-dispersion microprobe system. Operating conditions were: 2 mA, 15 kV, and 60 seconds counting time. The analytical uncertainty of chlorite is below 1%. Data reduction was carried out with an on-line Tracor Northern 5500 system, using the PRZ correction program.

Chlorite compositions and calculated  $T-f(O_2)$  conditions are given in Figures 2 and 3, respectively. A summary of representative data is given in Table 2. Stage-III chlorite is relatively enriched in iron [Mg numbers,  $100 Mg^{2+}/(Fe^{2+}+Fe^{3+}+Mg^{2+})$ , range from 20 to 28] compared with chlorite from Stages IV and V

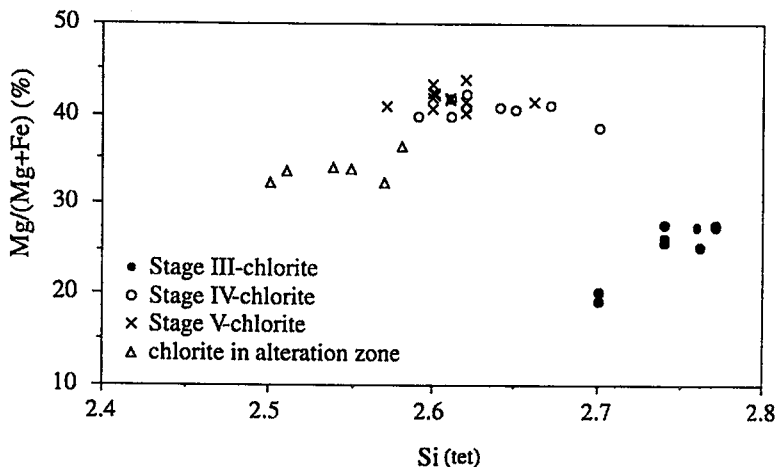


FIG. 2. Variation in magnesium number and silica content expressed as the content of  $Si^{4+}$  (in atoms per formula unit) in the tetrahedral site of different stages of chlorite from the veins and altered wallrock.

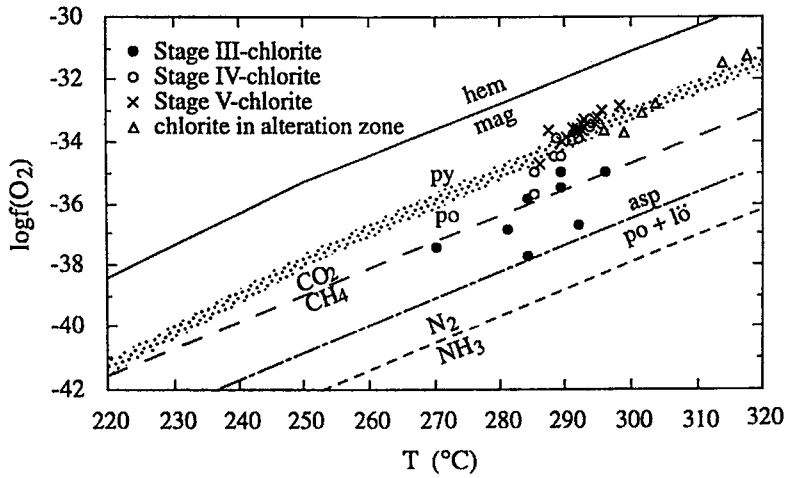


FIG. 3. Calculated temperatures and  $f(O_2)$  values for different types of chlorite from the veins and altered wallrock. Pyrite–pyrrhotite, magnetite–hematite and  $CO_2$ – $CH_4$  stability boundaries are plotted on the basis of data listed in Appendices I and II.

TABLE 2. CHLORITE COMPOSITIONS AND CONDITIONS OF FORMATION OF CHLORITE FROM THE HILL END GOLDFIELD

	III-chl	III-chl	III-chl	IV-chl	IV-chl	V-chl	V-chl	a-chl	a-chl
SiO <sub>2</sub>	24.05	23.81	24.33	24.47	24.12	24.48	24.39	22.77	23.36
Al <sub>2</sub> O <sub>3</sub>	18.17	19.61	18.72	20.14	21.20	20.76	21.15	21.61	20.85
FeO	36.58	38.88	39.08	30.54	30.42	30.35	29.68	32.47	31.12
MnO	0.20	0.20	0.28	0.13	0.23	0.36	0.35	0.37	0.46
MgO	6.89	5.13	5.40	11.59	11.22	11.88	11.95	8.98	9.73
Na <sub>2</sub> O	-	-	-	-	-	-	0.24	-	-
K <sub>2</sub> O	-	-	-	-	-	-	-	-	-
TiO <sub>2</sub>	-	0.13	-	-	-	-	-	-	-
Cr <sub>2</sub> O <sub>3</sub>	-	-	-	-	-	-	-	-	-
CaO	-	-	-	-	-	-	-	-	-
Total	85.89	87.76	87.81	86.87	87.19	87.83	87.76	86.20	85.52
Si(tet)	2.76	2.70	2.76	2.65	2.59	2.61	2.60	2.51	2.58
Mg#	25.44	19.38	20.22	40.50	39.94	41.50	42.18	33.53	36.39
T(°C)	290	295	280	290	295	290	290	315	300
logfO <sub>2</sub>	-35.4	-34.9	-36.8	-34.4	-33.4	-33.6	-33.4	-31.4	-33.6
logfS <sub>2</sub>	-11.9	-11.7	-12.9	-11.4	-10.9	-10.9	-10.8	-9.8	-11.0
loga <sub>H<sub>2</sub>S</sub>	-2.2	-2.1	-2.3	-2.5	-2.5	-2.5	-2.6	-2.4	-2.4
T(°C) <sup>1</sup>	305	325	305	310	315	315	315	330	320
T(°C) <sup>2</sup>	195	205	200	185	190	185	185	195	190

Analyses were performed using a JSM-840 scanning electron microprobe coupled with an energy-dispersion system under the conditions of 20 μA, 15 kV and 60 seconds counting time. All oxides expressed as wt%. Compositions are representative of Stages III-, IV- and V-chlorite from the veins, and chlorite from altered hostrock (a-chl). Mg# = 100 Mg/(Mg+Fe<sup>2+</sup>+Fe<sup>3+</sup>); T(°C)<sup>1</sup> = chlorite crystallization temperature calculated from the chlorite geothermometer of Cathelineau (1988); T(°C)<sup>2</sup> = as above, using chlorite geothermometer of Kranidiotis & MacLean (1987).

(Mg numbers range from 39 to 44, Fig. 2). The similar compositions displayed by Stage-IV and Stage-V chlorite are possibly due to recrystallization of Stage-IV chlorite during Stage-V activity, and the replacement of Stage-IV chlorite by Stage-V chlorite. Chlorite from the wallrocks has an intermediate compositions but is more aluminous than chlorite from the veins.

Calculated temperatures of chlorite crystallization fall within a range between 280 and 315°C. The Walshe (1986) geothermometer is sensitive to error in the analysis of the chlorite for silicon; a 1% error corresponds to a 10% error in the calculated temperature. For comparison, temperature calculations were also performed using the Cathelineau and Kranidiotis & MacLean geothermometers (De Caritat *et al.* 1993). Temperatures calculated using the Cathelineau (1988) geothermometer are 15–30°C higher than those obtained by the Walshe (1986) geothermometer. The Kranidiotis and MacLean (1987) geothermometer yielded much lower temperatures, in the range 185–205°C; this range is even lower than the raw data on homogenization temperature of the relevant fluid inclusions in quartz (Table 1, and Lu & Seccombe 1993). A detailed review of chlorite geothermometers by De Caritat *et al.* (1993) showed that in the temperature interval near 300°C, temperatures calculated using the Kranidiotis & Maclean (1987) geothermometer could be as low as 80°C below the measured temperature of chlorite formation (Fig. 6 of De Caritat *et al.* 1993). In contrast, the deviation between calculated temperature and measured temperature is within 10°C for the Walshe (1986) geothermometer.

At Hill End, chlorite precipitation occurred after the peak of metamorphism, during paragenetic stages III to V, implying that the temperature of chlorite precipitation is lower than 420°C. Fluid inclusion (Lu & Seccombe 1993) and stable isotope studies (Lu 1993) suggest that the mineralizing fluid is of metamorphic origin. Therefore, a pressure correction to the raw homogenization temperature (150–250°C, Table 1) is necessary. The results obtained from the Walshe (1986) geothermometer provide a basis for establishing the size of the pressure correction.

The inferred redox conditions for the crystallization of Stage-III chlorite are close to the CO<sub>2</sub>–CH<sub>4</sub> boundary (Fig. 3). In contrast, the fluids in equilibrium with Stage-IV and Stage-V chlorite and the wallrock chlorite seem to have been 1–2 log units above this boundary. Compared with the redox conditions implied by the composition of the gas phase in the relevant fluid inclusions, the calculated  $f(O_2)$  values are generally about 1 to 2 log units higher, especially the  $f(O_2)$  values calculated for Stage-IV chlorite. Most of the inclusions trapped in the Stage-IV event, corresponding to the deposition of Stage-IV chlorite, contain CH<sub>4</sub> as the dominant gas phase (Table 1 of Lu & Seccombe 1993). The more Al- and Fe-rich

character of the wallrock chlorite compared with chlorite in veins from Stages IV and V probably resulted from a higher value of  $a(Al^{3+})/a(H^+)$  in the wallrocks.

Calculated values of  $f(S_2)$  for Stage-III chlorite are consistent with the growth of chlorite in equilibrium with quartz and pyrrhotite. Calculated values of  $f(S_2)$  for Stage-III chlorite range between 1 and 5 log units below the pyrite–pyrrhotite buffer, implying that pyrrhotite is the only stable phase, consistent with the mineral assemblages of Stage III (Table 1). In contrast, calculated values of  $f(S_2)$  for Stage-IV and Stage-V chlorite and the wallrock chlorite range from about 2 log units below the pyrite–pyrrhotite buffer to about 1 log unit above the buffer. These conditions are consistent with growth of both pyrrhotite and pyrite during Stages IV and V. Calculated values for  $\log a(H_2S)_{aq}$  range between –2.2 to –2.3 for Stage-III fluids and between –2.5 and –2.6 for Stage-IV and Stage-V fluids.

Good agreement is obtained between the chlorite compositions indicated on Figure 3 and the position of chlorite in the paragenesis. The trend from low  $f(O_2)$  and an association with pyrrhotite for early chlorite, to higher  $f(O_2)$  and an association with pyrite, for chlorite formed later in the paragenesis, is clearly evident.

## DISCUSSION

### *An estimate of the pressure of formation of the deposit*

Calculated temperatures of chlorite formation for Stages III through V are consistently higher than homogenization temperatures for fluid inclusions from the same stages. Since both the homogenization temperatures and the chlorite temperatures are pressure-sensitive, the former more so than the latter, there is an opportunity to estimate a unique set of P–T conditions of mineralization.

A calculated P–T relationship for a portion of the system CH<sub>4</sub>–H<sub>2</sub>O<sub>(g)</sub>, where the concentration of CH<sub>4</sub> is taken to be 0.2 mole/kg H<sub>2</sub>O, is displayed on Figure 4. The CH<sub>4</sub> content of the fluid was calculated from the results of laser-Raman analysis of fluid inclusions (Lu & Seccombe 1993), based on the shift of the vibrational Raman frequency of CH<sub>4</sub> (Fabre & Oksengorn 1992), following the equation:

$$(P + n^2a/V^2)(V - nb) = nRT \quad (1)$$

in which the constants have values  $a = 2.25$ ,  $b = 0.04278$  and  $R = 0.08206$  atmosphere per mole per degree (Weast 1990). The bubble-point line of the CH<sub>4</sub>–H<sub>2</sub>O system ( $n_{CH_4} = 0.2$  mole/kg H<sub>2</sub>O) was established by Hanor (1980).

On Figure 4, points E and F are the lower-temperature limits calculated from the chlorite data under two different assumptions of confining pressure. Point F is

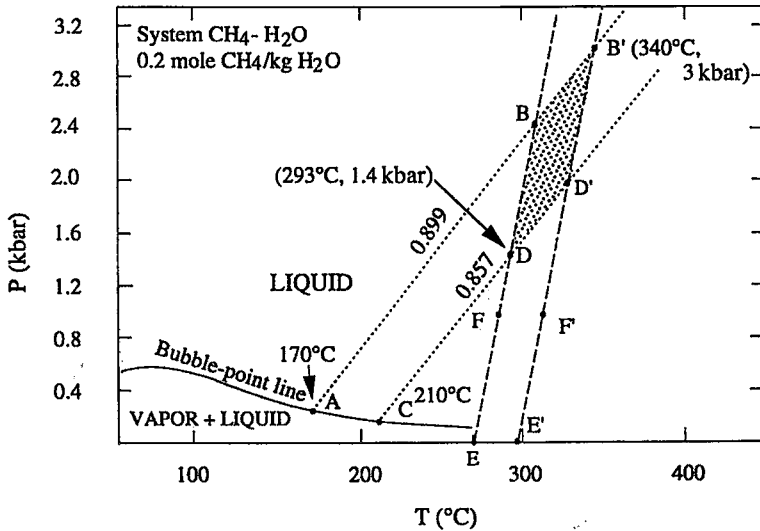


FIG. 4. Calculated P-T relations for a portion of the system  $\text{CH}_4\text{-CO}_2$ , where  $\text{CH}_4 = 0.2$  mole/kg  $\text{H}_2\text{O}$ . The shaded area is the estimated P-T regime for the Hill End fluids, which is confined by fluid-inclusion homogenization (Line AB' and line CD') and chlorite data (line BE and line BE').

calculated on the basis that the pressure remained constant at 1000 bars, whereas point E is calculated assuming that pressure followed the liquid-vapor curve for pure water, and line E-F represents the regression line for the pressure dependence of the temperature data calculated from chlorite compositions. Thus, the lower limits of the P-T data for chlorite crystallization are assumed to follow line E-F and its extrapolation through point B on Figure 4. Similarly, points E' and F' are the upper limits of the temperature data calculated from chlorite compositions under the same two assumptions concerning pressure, and line E'-B' defines the upper P-T limits for chlorite crystallization.

Fluid inclusions trapped during Stage III of the paragenesis (Table 1) demonstrate a range in  $T_h$  from 190 to 250°C, with a mode at 210°C (Lu & Seccombe 1993). Because the system involves  $\text{CH}_4$  rather than pure water, homogenization of a vapor-liquid inclusion takes place along the bubble-point line. For a temperature of homogenization of 210°C (point C on Fig. 4), the corresponding density isochor is 0.86. This means that the variation in P-T conditions of the fluid in the homogenized inclusion would follow line C-D, which intersects line B-E at point D, and intersects line B'-E' at point D'.

Fluid inclusions trapped during the later period of Stage-IV and Stage-V activity have a similar range in  $T_h$  from 150 to 190°C (Table 1); however, most of the data points are concentrated near 170°C (Lu & Seccombe 1993). Based on a similar reasoning as above, the variation of P-T conditions of the homogenized inclusions would follow line A-B, which

intersects line B-E at point B, and intersects line B'-E' at point B'. Therefore, the shaded area on Figure 4 is the estimated P-T regime of the Hill End fluids, which gives a range in pressure from 1.4 to 3 kbar and a range in temperature from 295 to 340°C.

The above estimated temperatures provide a means of establishing the extent of the temperature correction for the fluid-inclusion  $T_h$  data from coexisting quartz. Stage-III chlorite precipitated in the middle to late parts of the Stage-III paragenesis.  $T_h$  values of fluid inclusions trapped in quartz during this period are in the range 190-250°C. If the temperature range 295-340°C determined from Figure 4 is taken as the estimated true temperature of the fluid, then a temperature correction to the  $T_h$  data between 45 and 150°C may be envisaged for this generation of fluid inclusions.

By a similar argument, a temperature correction of about 45-150°C may be inferred for  $T_h$  data in the range 190-250°C represented by inclusions trapped during Stage IV of fluid activity. Also,  $T_h$  data that range between 150 and 190°C for primary fluid inclusions trapped during Stage V may require a temperature correction of about 100-190°C to be consistent with the range in temperature of 295-340°C calculated for Stage-V chlorite.

Explanations for the variation in the magnitude of the temperature correction for the different generations of fluid inclusions are likely to be both geological and chemical: (1) The lithostatic load on the vein systems has varied during mineralization. This is indicated by the vein structures, which display a change from a

ductile to a brittle structural regime during the evolution of the veins. This is particularly true if we consider the pressure variation likely to be encountered during "crack-seal" (Ramsay 1980) cycles of vein accumulation. In addition, textural evidence of the post-lamination nature of Stage-V quartz shows that the final-stage fluid has been subjected to a quite different environment of pressure compared with the previous stages of fluid activity. The coarse-grained, vuggy Stage-V quartz encountered at the crest of the anticline displays open-space infilling textures. Differing pressures will result in significant differences in the corresponding temperature-correction for  $T_h$  data (Potter 1977). (2) The chemical properties of the inclusion fluids vary significantly. Although all inclusions contain a low-salinity aqueous fluid, major differences exist among the several stages of fluids according to the amounts of dissolved gases. The presence of variable amounts of  $N_2$ ,  $CH_4$ , or  $CO_2$  will have a significant effect on the position of the solvus of low-salinity aqueous fluids (Hollister & Burruss 1976, Bowers & Helgeson 1983). In addition, isochors for  $CO_2$ -rich fluids will be different from those established for  $CH_4$ - $H_2O$  and  $H_2O$ -based systems (Roedder 1984), resulting in differing temperature-corrections for any given pressure. Both of these factors will affect the magnitude of the temperature correction, but the extent is difficult to quantify.

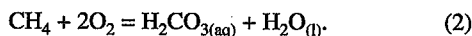
Uncertainties exist in interpreting the temperatures calculated from the composition of chlorite. The possibly lengthy time-intervals indicated by some of the paragenetic stages produce difficulties in precisely correlating periods of quartz deposition with periods of chlorite deposition. Also, because individual fluid inclusions developed in quartz cannot be related directly to the precipitation of chlorite, only average  $T_h$  data can be employed in a comparison of temperatures derived from fluid inclusions with those obtained from the composition of chlorite. Nevertheless, with careful paragenetic control, the chlorite geothermometer seems capable of resolving some of the uncertainties in the study of multistage fluid-dominated systems, especially since it offers an independent check of temperature data generated by fluid-inclusion studies in metamorphic environments.

#### *Physicochemical conditions of mineralization*

The stages of mineralization at Hill End can be defined by considering phase equilibria involving mineral and fluid, using fluid parameters established from fluid inclusions, chlorite compositions and mineral paragenesis. For a temperature of 300°C (within the temperature interval for the gold deposition as estimated from Fig. 4), the stability fields of aqueous sulfur species may be computed as functions of pH and  $\log f(O_2)$ .

The total sulfur content of the fluid ( $\Sigma S$ ) may be estimated from  $H_2S$  concentration in the fluid [ $\log \alpha(H_2S)_{aq}$  ranges from -2.16 to -2.64; Table 1]. A value for  $\Sigma S$  of  $2 \times 10^{-2}$  mol/kg is obtained, by assuming 1) an ionic strength of one, and 2) the mole fraction of  $H_2S_{(aq)}$  [ $XH_2S_{(aq)}$ ] nearly equal to  $\Sigma S$ . The second assumption is based on the observation that pyrrhotite and pyrite are the dominant sulfides, and the calculated  $\log f(O_2)$  values from the composition of chlorite are mostly below or close to the pyrite-pyrrhotite buffer (Fig. 3). This finding implies that  $H_2S$  is the major species of dissolved sulfur in the fluid (Ohmoto & Rye 1979). In constructing a diagram to define the stability fields of mineral species present in the auriferous quartz veins, Fe-O-S mineral boundaries were computed as functions of pH and  $\log f(O_2)$  under the conditions of  $T = 300^\circ C$ , ionic strength = 1 and  $\Sigma S = 2 \times 10^{-2}$  mol/kg (Fig. 5). All of the equations and the relevant equilibrium constants and ionic activity coefficients used in these calculations are listed in Appendices I and II, respectively. The stability field for the mineral assemblages precipitated during episodes of gold mineralization (the shaded area) is constrained by using the fluid parameters established from fluid-inclusion data, chlorite data and mineral paragenesis.

Because the ratio of  $CH_4$  to  $CO_2$  changes significantly in the inclusion fluids during mineralization, the  $CO_2$ - $CH_4$  boundary on Figure 5 was established using data in Appendix II and the following equation:



At a temperature of 300°C, the  $CO_2$ - $CH_4$  boundary lies at  $f(O_2) = 10^{-34.9}$ . Ohmoto (1986) stressed that disequilibrium is common between  $CO_2$  and  $CH_4$  below 250°C, which is likely to have been only 50–90°C less than the estimated temperature of the ore fluids at Hill End. The validity of using the calculated stability-boundary between  $CH_4$  and  $CO_2$  therefore may be questioned. However, the plotted position of this boundary agrees well with the results obtained in our study, on the basis of both fluid-inclusion evidence and  $f(O_2)$  values calculated from the chlorite data.

The lower limit of the  $f(O_2)$  prevailing in the mineralizing fluids is based on the value calculated from the chlorite composition and also the composition of arsenopyrite developed in the country rocks. From Figure 5, the lowest  $f(O_2)$  value obtained from the chlorite data is located at about 1.8 log units below the  $CO_2$ - $CH_4$  boundary. At a temperature of 300°C, the  $CO_2$ - $CH_4$  boundary is located at a  $f(O_2)$  value of  $10^{-34.9}$ , which implies that the lowest  $f(O_2)$  value in the fluid could have been as low as  $10^{-36.7}$ . This value is almost the same as the  $f(O_2)$  value calculated from the arsenic content of the arsenopyrite (Kretschmar & Scott 1976). On Figure 5, the calculated arsenopyrite-löllingite boundary is located at a  $f(O_2)$  value of  $10^{-36.4}$ .

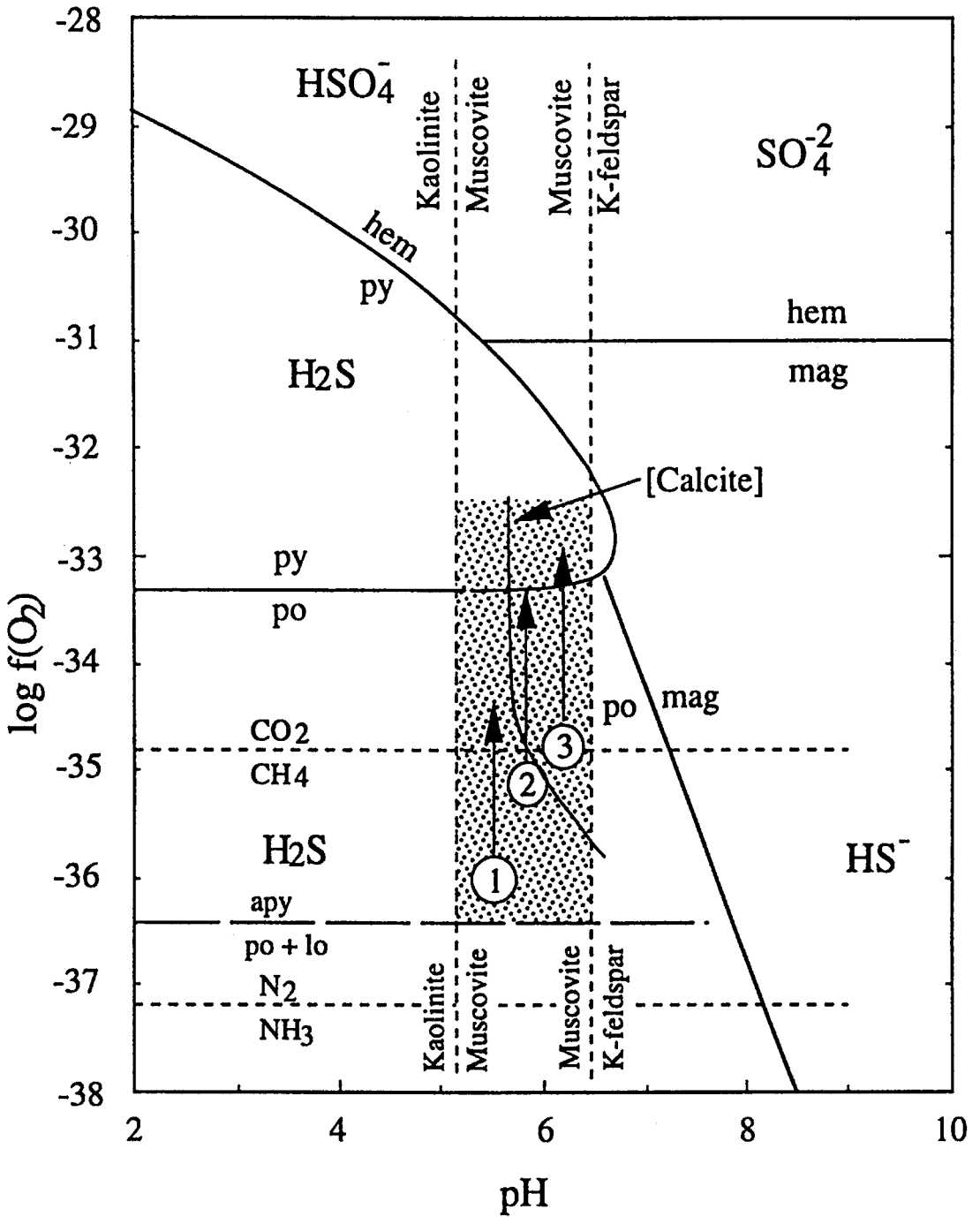


FIG. 5.  $\log f(\text{O}_2)$ -pH diagram giving the stability fields for minerals in the system Fe-O-S, relative to mineral and dissolved gas buffers, and fields of dominant aqueous species of sulfur. Numbered arrows indicate likely paths of fluid evolution during the three stages of gold deposition. Diagram established for  $T = 300^\circ\text{C}$ ,  $\Sigma S = 0.002 \text{ mol/kg}$  and ionic strength = 1.0.

corresponding to an arsenopyrite composition of 45 wt% As.

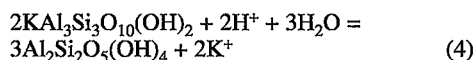
This result also is consistent with the redox conditions implied by the composition of the gas phase in fluid inclusions. N<sub>2</sub> is the only gas phase encountered in fluid inclusions from Stage I of fluid activity. Since NH<sub>3</sub> is not detected in any inclusion fluids, the redox conditions therefore must be located above the N<sub>2</sub>-NH<sub>3</sub> boundary, which can be calculated from:



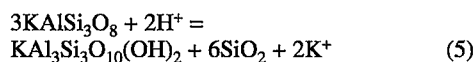
where logK at 300°C is taken from Johnson *et al.* (1992).

The upper limit of  $f(\text{O}_2)$  for the mineralization is constrained by the composition of chlorite associated with pyrite. From Figure 5, some Stage-V chlorite is located above the pyrite-pyrrhotite buffer by about one log unit; the pyrite-pyrrhotite buffer is located at a log  $f(\text{O}_2)$  value of -33.3, and the upper limit for the redox conditions is approximately constrained at a log  $f(\text{O}_2)$  value of -32.3.

The pH range during mineralization is deduced from the presence of muscovite and the absence of either K-feldspar or kaolinite in the hydrothermal assemblages. Boundary conditions are set by:



and



The molar concentration of K<sup>+</sup> has been determined from the bulk analysis of inclusion fluids extracted from several samples of pulverized vein quartz, where attempts were made to select single generations of quartz for analysis (Lu & Seccombe 1993). The concentration of K<sup>+</sup> in these fluids ranges from 0.31 to 0.56 mg/g (average 0.35 mg/g). Using these figures, calculated values of pH for the mineralizing fluids range from 5.2 to 6.4. Equilibrium constants required in these calculations come from the data of Helgeson (1969).

Fluid-evolution lines are indicated on Figure 5 by the numbered arrows. For the first episode of gold mineralization (path 1), during Stage-III fluid activity, the calculated log  $f(\text{O}_2)$  values of Stage-III chlorite, which precipitated in the middle to late stages of this fluid-circulation event, range from below the CO<sub>2</sub>-CH<sub>4</sub> boundary to slightly above this line. This position indicates that the redox conditions are mainly confined to the methane field during the early to middle stages, consistent with the presence of CH<sub>4</sub> in fluid inclusions trapped in quartz at this stage. The associated iron

sulfide is invariably pyrrhotite. Minor amounts of calcite are deposited in the late stage of this event, possibly associated with the development of late chlorite, at a time when redox conditions moved up to CO<sub>2</sub>-CH<sub>4</sub> boundary.

Path 2 (Fig. 5) traces the pH and log  $f(\text{O}_2)$  variation in the second episode of gold mineralization (Stage IV). Although all the calculated  $f(\text{O}_2)$  data pertinent to Stage-IV chlorite define a fluid composition above the CO<sub>2</sub>-CH<sub>4</sub> boundary (Fig. 3), the relevant fluid inclusions trapped in this stage contain CH<sub>4</sub> as the major gas phase. This may indicate that in the early stages of this event, the redox condition of the fluid is confined to the stability field of methane. Part of the  $f(\text{O}_2)$  data for Stage-IV chlorite are below or close to the pyrite-pyrrhotite buffer (Fig. 3), but several data points are above this buffer. Therefore, on Figure 5, the redox condition at this stage of evolution of the fluid covers the field defined by the presence of CO<sub>2</sub> in the fluid phase and pyrrhotite as the stable iron sulfide, but ultimately enters the stability field of pyrite. This agrees with the mineral assemblages in which pyrrhotite is the dominant sulfide, and pyrite only appears in the very latest stage of this second episode of gold deposition.

The Stage-V chlorite, which crystallized over a  $f(\text{O}_2)$  range close to and above the pyrite-pyrrhotite buffer, defines the evolution of fluid in the late stages of the last episode of gold deposition. In the early stages of this last event, Stage-V quartz was deposited while trace amounts of CH<sub>4</sub> still existed in the fluid. This indicates that the redox conditions remained near the CO<sub>2</sub>-CH<sub>4</sub> boundary. Toward the middle to late stages of this final event, CO<sub>2</sub> became the major gas phase in the fluid inclusions, and Stage-V chlorite precipitated with pyrrhotite under redox conditions below the pyrrhotite-pyrite buffer. In the last stages of gold deposition, the redox conditions in the fluid became relatively oxidizing and moved above the pyrrhotite-pyrite buffer. Pyrite became the dominant sulfide. Stage-V chlorite crystallized together with pyrite and calcite, and apparently coincided with the appearance of some liquid-CO<sub>2</sub>-bearing fluid inclusions in the latest Stage-V quartz in the hinge zone of the Hill End anticline.

## CONCLUSIONS

Temperatures calculated from chlorite compositions at each paragenetic stage combined with the homogenization temperature of fluid inclusions in associated quartz should provide a relatively reliable check on inferred temperatures of trapping obtained from the fluid inclusions. This is particularly so because the performance of the chlorite model appears to be well established by the consistency between the calculated  $f(\text{O}_2)$  and  $f(\text{S}_2)$  data and the nature and paragenetic position of the vein assemblages. This

consistency is supported at least in part by the data obtained for gas species in the fluid inclusions.

The average corrections to  $T_h$  data provided by the chlorite model are estimated to be about 45–150°C for the inclusions trapped during Stage-III fluid activity, 90–150°C for the inclusions trapped in the Stage-IV event, and 100–190°C for the inclusions trapped in the last stage (Stage V), respectively.

The calculated redox parameters for each particular stage of mineralization, combined with fluid-inclusion data and mineral assemblages, can be summarized as follows: 1)  $f(O_2)$  ranged from  $10^{-36.4}$  to  $10^{-34}$  in the first episode of gold mineralization (Stage III). Under these conditions,  $CH_4$  is the dominant carbon species in the fluid inclusions, and pyrrhotite is the only sulfide. 2) During the second episode of gold mineralization (Stage IV of the paragenesis),  $f(O_2)$  remained between  $10^{-35.6}$  and  $10^{-33.4}$ . Early in this stage,  $CH_4$  was the dominant gaseous species in the fluid inclusions, and pyrrhotite was the dominant sulfide. 3) The redox environment changed dramatically during the last episode of gold mineralization. At that stage,  $f(O_2)$  ranged from  $10^{-34.7}$  to  $10^{-32}$ ,  $CO_2$  gradually became the dominant gaseous species in fluid inclusions, and pyrite became the dominant sulfide.

Despite some uncertainties, with careful paragenetic control, the chlorite geothermometer seems to be a powerful tool in deciphering multistage fluid systems, and offers a solution to some of the ambiguities attending fluid-inclusion studies in metamorphic environments.

#### ACKNOWLEDGEMENTS

We thank the management and staff of Silver Orchid Limited, especially Robert Cleaver, Barry and Hilary Montgomery and Alan Dennington for hospitality and support during sampling at Hill End. D. Phelan and G. Weber are thanked for their help with extensive periods of microprobe analysis. B. Harrold and Z. Jiang are thanked for their assistance with computing. Technical assistance provided by R. Bale, J. Crawford, E. Krupic and H. Nesmith at the University of Newcastle is greatly appreciated. Financial assistance for this research was provided by grants from the University of Newcastle, CSIRO and the government of Australia through an Overseas Postgraduate Research Scholarship to Jianchun Lu. Constructive and careful reviews by E.D. Ghent and an anonymous referee greatly improved the presentation of our findings.

#### REFERENCES

- AHMAD, M., SOLOMON, M. & WALSH, J.L. (1987): Mineralogical and geochemical studies of the Emperor gold telluride deposits, Fiji. *Econ. Geol.* **82**, 345-370.
- BOWERS, T.S. & HELGESON, H.C. (1983): Calculations of the thermodynamic and geochemical consequences of nonideal mixing in the system  $H_2O-CO_2-NaCl$  on phase relations in geological systems: equation of state for  $H_2O-CO_2-NaCl$  fluids at high pressures and temperatures. *Geochim. Cosmochim. Acta* **47**, 1247-1275.
- CATHELIN, M. (1988): Cation site occupancy in chlorites and illites as a function of temperature. *Clay Minerals* **23**, 471-485.
- CRERAR, D.A. & BARNES, H.L. (1976): Ore solution chemistry. V. Solubilities of chalcopyrite and chalcocite assemblages in hydrothermal solution at 200°C to 300°C. *Econ. Geol.* **71**, 772-794.
- DE CARITAT, T.P., HUTCHISON, I. & WALSH, J.L. (1993): Chlorite geothermometry: A review. *Clays Clay Minerals* **41**, 219-239.
- FABRE, D. & OKSENGORN, B. (1992): Pressure and density dependence of the  $CH_4$  and  $N_2$  Raman lines in an equimolar  $CH_4/N_2$  gas mixture. *Applied Spectroscopy* **46**, 468-471.
- HAAS, J.L., JR. & ROBIE, R.A. (1973): Thermodynamic data for wustite,  $Fe_{0.947}O$ , magnetite,  $Fe_3O_4$ , and hematite,  $Fe_2O_3$ . *Am. Geophys. Union Trans.* **54**, 483 (abstr.).
- HANOR, J.S. (1980): Dissolved methane in sedimentary brines: potential effect on the PVT properties of fluid inclusions. *Econ. Geol.* **75**, 603-609.
- HARPER, L.F. (1918): The Hill End - Tambaroora Gold-Field. *New South Wales Dep. Mines, Geol. Surv., Mineral Resources* **27**, 74.
- HELGESON, H.C. (1969): Thermodynamics of hydrothermal systems at elevated temperatures and pressures. *Am. J. Sci.* **267**, 729-804.
- , DELANY, J.M., NESBITT, H.W. & BIRD, D.K. (1978): Summary and critique of the thermodynamic properties of rock-forming minerals. *Am. J. Sci.* **278-A**.
- & KIRKHAM, D.A. (1974): Theoretical prediction of the thermodynamic behaviour of aqueous electrolytes at high pressures and temperature. 1. Summary of the thermodynamic/electrostatic properties of the solvent. *Am. J. Sci.* **274**, 1089-1198.
- HOLLISTER, L.S. & BURRUS, R.C. (1976): Phase equilibria in fluid inclusions from Khtada Lake metamorphic complex. *Geochim. Cosmochim. Acta* **40**, 163-175.
- JOHNSTON J.W., OELKERS, E.H. & HELGESON, H.C. (1992): SUPRC92: a software package for calculating the standard molal thermodynamic properties of minerals, gases, aqueous species, and reactions from 1 to 5000 bar and 0 to 1000°C. *Comput. Geosci.* **18**, 899-947.
- KRANIDIOTIS, P. & MACLEAN, W.H. (1987): Systematics of chlorite alteration at the Phelps Dodge massive sulfide deposit, Matagami, Quebec. *Econ. Geol.* **82**, 1898-1911.
- KRETSCHMAR, U. & SCOTT, S.D. (1976): Phase relations involving arsenopyrite in the system  $Fe-As-S$  and their application. *Can. Mineral.* **14**, 364-386.

- LU, JIANCHUN (1993): *Geochemical Studies of a Turbidite-Hosted Auriferous Vein System, Hill End Goldfield, NSW, Australia*. Ph.D. thesis, Univ. of Newcastle, Callaghan, Australia.
- & SECCOMBE, P.K. (1993): Fluid evolution in a slate-belt gold deposit: a fluid inclusion study of the Hill End goldfield, NSW, Australia. *Mineral. Deposita* **28**, 310-323.
- NAUMOV, G.B., RYZHENKO, B.N. & KHODAVOSKY, I.L. (1974): *Handbook of Thermodynamic Data*. U.S. Dep. Commerce, Nat. Tech. Inf. Serv.
- OFFLER, R. & PRENDERGAST, E. (1985): Significance of illite crystallinity and  $b_0$  values of K-white mica in low grade metamorphic rocks, North Hill End Synclinorium, New South Wales, Australia. *Mineral. Mag.* **49**, 357-364.
- OHMOTO, H. (1986): Stable isotope geochemistry of ore deposits. *Rev. Mineral.* **16**, 491-560.
- & RYE, R.O. (1979): Isotopes of sulfur and carbon. In *Geochemistry of Hydrothermal Ore Deposits* (H.L. Barnes, ed.). Wiley Interscience, New York, N.Y. (509-567).
- PACKHAM, G.H. (1969): Southern and central Highlands fold belt. In *The Geology of New South Wales* (G.H. Packham, ed.). *J. Geol. Soc. Aust.* **16**, 73-226.
- POTTER, R.W., II (1977): Pressure correction for fluid-inclusion homogenization temperatures based on the volumetric properties of the system NaCl-H<sub>2</sub>O. *U.S. Geol. Surv. J. Res.* **5**, 603-607.
- POWELL, C.MCA. (1976): Geology of the Hill End Trough and Molong High: a critical reappraisal of the tectonic history of the Hill End Trough and its margins. *Bull. Aust. Soc. Explor. Geophys.* **7**, 14-18.
- & EDGECOMBE, D.R. (1978): Mid-Devonian movements in the north eastern Lachlan Fold Belt. *J. Geol. Soc. Aust.* **25**, 165-184.
- PRENDERGAST, E. (1981): *The Biotite Isograd of the Northern Hill End Trough Succession*. B.Sc. Hons. thesis, Macquarie Univ., Sydney, Australia.
- RAMSAY, J.G. (1980): The crack-seal mechanism of rock deformation. *Nature* **284**, 135-139.
- RIPLEY, E.M. & OHMOTO, H. (1977): Mineralogical, sulfur isotope, and fluid inclusion studies of the stratabound copper deposits at the Raul mine, Peru. *Econ. Geol.* **72**, 1017-1041.
- ROEDDER, E. (1984): Fluid inclusions. *Rev. Mineral.* **12**.
- SCHIEBNER, E. (1973): A plate tectonic model of the Palaeozoic tectonic history of New South Wales. *J. Geol. Soc. Aust.* **20**, 405-426.
- SECCOMBE, P.K. & HICKS, M.N. (1989): The Hill End Goldfield, NSW, Australia - early metamorphic deposition of auriferous quartz veins. *Mineral. Petrol.* **40**, 257-273.
- , LU, JIANCHUN, ANDREW, A.S., GULSON, B.L. & MIZON, K.J. (1993): Nature and evolution of metamorphic fluids associated with turbidite-hosted gold deposits: Hill End goldfield, NSW, Australia. *Mineral. Mag.* **57**, 423-436.
- SMITH, R.E. (1969): Zones of progressive regional burial metamorphism in part of the Tasman Geosyncline, Eastern Australia. *J. Petrol.* **10**, 144-163.
- WALSHE, J.L. (1986): A six-component chlorite solid solution model and the conditions of chlorite formation in hydrothermal and geothermal systems. *Econ. Geol.* **81**, 681-703.
- WEAST, R.C., ed. (1990): *Handbook of Chemistry and Physics* (70th edition). CRC Press, Cleveland, Ohio.
- WINDH, J. (1990): Structural constraints on saddle reef gold-quartz vein genesis, Hill End goldfield, New South Wales, Australia. *Int. Assoc. Genesis Ore Deposits, 8th Symp., Program Abstr.*, 152-153.

Received November 15, 1994, revised manuscript accepted September 16, 1995.

APPENDIX I. EQUILIBRIUM CONSTANTS FOR REACTIONS IN THE Fe-O-S-H<sub>2</sub>O SYSTEM

		logK <sub>T</sub>			Ref.
		200°C	250°C	300°C	
1.	$\text{H}_2\text{O(l)} = \text{H}^+ + \text{OH}^-$	-11.27	-11.13	-11.39	a
2.	$\text{H}_2\text{S(aq)} = \text{H}^+ + \text{HS}^-$	-6.96	-7.35	-8.06	a
3.	$2\text{H}_2\text{S(aq)} + \text{O}_2(\text{g}) = 2\text{H}_2\text{O(l)} + \text{S}_2(\text{g})$	35.3	31.0	27.4	b
4.	$2\text{H}^+ + \text{SO}_4^{2-} = \text{H}_2\text{S(aq)} + 2\text{O}_2(\text{g})$	-64.13	-57.10	-48.55	a
5.	$\text{HSO}_4^- = \text{H}^+ + \text{SO}_4^{2-}$	-4.49	-5.41	-7.06	a
6.	$\text{KSO}_4^- = \text{K}^+ + \text{SO}_4^{2-}$	-1.94	-2.60	-3.18	c
7.	$\text{NaSO}_4^- = \text{Na}^+ + \text{SO}_4^{2-}$	-1.94	-2.60	-3.18	c
8.	$\text{CaSO}_4(\text{aq}) = \text{Ca}^{2+} + \text{SO}_4^{2-}$	-3.6	-4.0	-4.50	g
9.	$2\text{FeS}_2 = 2\text{FeS} + \text{S}_2(\text{g})$	-16.56	-13.46	-10.91	d
10.	$3\text{FeS}_2 + 2\text{O}_2(\text{g}) = \text{Fe}_3\text{O}_4 + 3\text{S}_2(\text{g})$	37.7	35.5	33.6	e
11.	$6\text{Fe}_2\text{O}_3 = 4\text{Fe}_3\text{O}_4 + \text{O}_2(\text{g})$	-40.5	-35.3	-31.0	f

Sources: a. Helgeson (1969); b. logK from Ahmad et al. (1987), data for H<sub>2</sub>S(aq) from Naumov et al. (1974) and H<sub>2</sub>O from Helgeson & Kirkham (1974); c. logK from Ripley & Ohmoto (1977), based on data from Helgeson (1969) and extrapolated above 200°C, dissociation constant for NaSO<sub>4</sub><sup>-</sup> assumed equal to the dissociation constant for KSO<sub>4</sub><sup>-</sup>; d. Crerar & Barnes (1976) using data from Scheibner (1973); e. logK from Ahmad et al. (1987), based on data from Helgeson et al. (1978); f. Ripley & Ohmoto (1977), based on data from Haas & Robie (1973); g. Helgeson (1969), extrapolation above 200°C.

## APPENDIX II. ACTIVITY COEFFICIENTS OF IONS CONSIDERED\*

Species	Temperature (°C)		
	200	250	300
K <sup>+</sup>	-0.34	-0.42	-0.59
HS <sup>-</sup> , OH <sup>-</sup> ,	-0.31	-0.38	-0.51
S <sup>2-</sup>	-1.08	-1.30	-1.63
SO <sub>4</sub> <sup>2-</sup>	-1.25	-1.50	-1.87
HSO <sub>4</sub> <sup>-</sup> , HCO <sub>3</sub> <sup>-</sup> , NaSO <sub>4</sub> <sup>-</sup> , KSO <sub>4</sub> <sup>-</sup>	-0.28	-0.35	-0.47
Ca <sup>2+</sup>	-0.96	-1.15	-1.45
CH <sub>4</sub> , H <sub>2</sub> S, H <sub>2</sub> CO <sub>3</sub>	0.99	0.12	0.20
CO <sub>3</sub> <sup>2-</sup>	-1.16	-1.39	-1.74

From Ahmad et al. (1987) calculated following procedures given in Helgeson (1969). Ionic strength = 1.

\* Expressed as logarithms to base 10.